doi:10.3166/acsm.40.131-142 © Lavoisier, Paris
Thermal spray process *Ann. Chim. Sci. Mat.*, 2016, 40 (3-4), pp. 131-142

MICROSTRUCTURE AND INTERFACIAL STRENGTH OF STAINLESS STEEL COATINGS OBTAINED BY THERMAL SPRAY PROCESS.

Abdellah SADKI[1], Rassim YOUNES[2], Mohand Amokrane BRADAI[2],
Mohamed Lamine HATTALI[3], Nadir MESRATI[1,4]

[1] Laboratory of Sciences and Materials Engineering, National Polytechnic School of Algiers. Algiers (Algeria).
[2] Laboratory of Mechanics, Materials and Energetic, Faculty of Technology, University of Bejaia, Algeria.
[3]Laboratory Fluid Automation and Thermal Systems - Bat. 502 University campus- 91405 Orsay Cedex (France).
[4] Higher School of Aeronautical Technical, Dar El Beida Alger.

Abstract. The present investigation has been conducted to study the adhesion of X10CrMnNi18-8-5 austenitic stainless steel (ASTM 301) coatings deposited on two different substrates of aluminum alloys such as AG3 (ASTM 5754) and AU4G (ASTM 2017A) by using arc spraying process (APS). The structure, microstructure and phase composition coatings were analyzed by SEM, EDS and XRD. The adhesion tests were carried out using 4-point bending tests. The SEM showed that the dense microstructures of ASTM 301 coatings have a homogeneous lamellar morphology with the presence of porosities and unmelted particles. The XRD spectrum of coatings revealed the main phase corresponding the solid solution as face-centered cubic (fcc) structure and also the presence of small proportion of the metastable form γ-Fe2O3 and FeO oxides. The microhardness of coatings is near four times than the two substrates of aluminum alloys. The 4-point bending tests results showed that the critical interfacial fracture energy GIC of the composite system B namely (ASTM 2017A/75E bond coat/ASTM 301) is three times greater than the composite system A (ASTM 5754/75E bond coat/ASTM 301).

Résumé. Microstructure et adhérence interfaciale des revêtements en acier inoxydable obtenus par projection thermique. La présente étude a pour objectif d'étudier l'adhérence des revêtements en acier inoxydable austénitique type X10CrNi18-8 (ASTM 301) déposés sur deux substrats différents d'alliages d'aluminium tels que: AG3 (ASTM 5754) et AU4G (ASTM 2017A) en utilisant le procédé de projection thermique à arc électrique. La structure, la microstructure et les compositions des différentes phases des revêtements obtenus ont été analysés par MEB, EDAX et DRX. Les essais d'adhérence ont été effectués en utilisant des essais de flexion quatre points. Les résultats MEB ont montré que les microstructures des revêtements (ASTM 301) sont denses et présentent une morphologie lamellaire homogène avec la présence de porosités et de particules non fondues. Le spectre DRX des revêtements en acier inoxydable révèle une phase principale correspondant à la solution solide de structure cubique à faces centrées (CFC) et la présence d'une faible proportion de la forme métastable γ-Fe2O3 et des oxydes type FeO. Les valeurs de microdureté des revêtements sont pratiquement quatre fois supérieures à celles des deux substrats d'alliages d'aluminium. Les résultats des essais de flexion quatre points ont montré que l'énergie de rupture interfaciale GIC du système composite B (substrat ASTM 2017A / sous couche d'accrochage 75E / dépôt ASTM 301) est trois fois supérieure au système composite A (substrat ASTM 5754 / sous couche d'accrochage 75E / dépôt ASTM 301).

1. INTRODUCTION

Thermal spraying is one kind of surface engineering technologies which is utilized in almost industrial fields. Continuous advancements and enhanced understanding of thermal spray technology has facilitated a synergetic approach towards a sustainable growth of its industrial applications.The arc spraying process (ASP) is a technique that produces a wide range of coatings for diverse applications; it allows combining properties resist to wear [1-4], corrosion [5] and thermal insulation [6-7]. However, the adhesion of such coatings to the substrate generates stress at the interface [8-11]. The electric arc-spraying process can be used to effectively deposit surface coatings that have superior hardness, corrosion resistance and wear resistance. In addition to these advantages, the spray parameters (voltage, current, air pressure and spray distance) of the electric arc spray process can be optimized for specific application.

Aluminum alloys have been enormously used in aerospace and automobile industries due to superior properties, such as high specific strength, excellent low-temperature performance, exceptional corrosion resistance, chemical inertness [12]. However, the poor performance and wear resistance are the main weaknesses of aluminum alloys. To settle these problems, aluminum alloys coated by austenitic stainless have been developed. The wear resistance of this material was improved [13-14], and possibly in biomedical fields [15, 16].

Stainless steel is one of the most widely used steel alloys containing chromium. Its superior properties, such as its excellent mechanical strength and offers great applicability due to its attractive appearance, wear resistance, major appliances, construction, surgical instruments, automotive parts, and aerospace engineering. The adhesion of stacked lamellae coating in advanced devices has become important characteristics of the mechanical properties concerned characteristic.

The interfacial strength phenomenon is degradable to mechanical reliability when several stacked lamellae used in device structures are introduced. Thus, interfacial adhesion of a coatings to the substrates can be quantified by different techniques should be widely developed [17, 18]. Several methods, such as blister test [19], nano-indentation [20-22], modified decohesion test [23], nanoscratch test [24, 25], double cantilever beam test [26,27], laser spallation test [28, 29] and four-point bending test (4PBT) [30-41].

The aim of the present work is to produce austenitic stainless steel ASTM 301 (X10CrMnNi18-8-5) coatings using an arc spray process (APS). These coatings were deposited onto two different substrates which used in aeronautical industries such as ASTM 5754 and ASTM 2017A in order to enhance a good mechanical strength on the aluminum alloy substrates. In this goal, two types of composite systems, A and B, have been prepared: (A) (ASTM 5754/75E bond coat/ASTM 301) and (B) (ASTM 2017A/75 E bond coat/ASTM 301). The structure, microstructure and phase composition coatings were analyzed by scanning electron microscope (SEM), electron dispersive Spectroscopy (EDS) and X-ray diffraction (XRD). Measurements of profil micro hardness were performed on the surface of the two composite systems. The adhesion tests were carried out using 4-point bending tests in order to determine interfacial strength of stainless steel coatings.

2. EXPERIMENTAL DETAILS

2.1. Materials and spraying parameters

The present investigation has been carried out employing two substrates based aluminium with different chemical composition. This chemical composition was obtained by using analysis X-rays fluorescence which is shown in *Table 1*.

Before the coating process, the surface of the substrate was grit blasted with corundum particles of 99,50 wt % purity and 0,5 mm mean particle size, using an air of 0,4MPa, an incidence angle of 90° and a gun-to-substrate distance of 150 mm. The surface was then cleaned and degreased using acetone within an ultrasonic bath. The grit blasted substrates was carried out in

order to increase the surface roughness of the samples and improve the mechanical bonding of the coating to be deposited.

Table 1: Chemical composition of substrates.

Elements	Al %	Cu %	Cr %	Mn %	Mg %
ASTM 2017A	94.3	4	0.5	0.5	0.7
ASTM 5754	96.3	-	0.3	0.3	3.1

The surface roughness of the grit blasted specimens was found to increase from Ra ~0.09 µm to Ra ~3.33µm *(Table.2)*. Specimens were located at a distance of approximately 140 mm from the gun and the blasting process was conducted at a mean pressure of 300 KPa. Different sizes of aluminum alloys were machined according to the tests to be performed as 65×15×2.5 mm^3 rectangular substrates were machined for the 4-point bending adhesion tests.

Table 2. Roughness of different materials used.

Substrate	Brut state Ra (µm)	Polished state Ra (µm)	Grit blasted state Ra (µm)
ASTM 2017A	1.21	0.09	2.87
ASTM 5754	1.84	0.1	3.33

Table 3. Chemical composition of different materials used.

Elements	Al	Ni	Cr	Mn	Fe
Bond coat 75E	19.4	79.2	/	/	/
Coating ASTM 301	-	5	18	8	Balance

The roughness measurements to determine surface roughness profile of each substrate were made with a profilometry (Hommel tester T500). It is optical metrology equipment used to study surface topography. It is carried out over 25 mm stylus tracing length, collecting 14000 data points per measurement. With the aim to remove the natural oxide layer presented on the substrate surface, which acts as a diffusion barrier, some aluminum alloy substrates were immersing during 3 minutes at 80°C in alkaline solution of sodium zincate.

Table 4. Thermal spray operating parameters

Projection parameters	X10CrNi18-8
Air pressure in the engine (bars)	3.8
Air pressure in the spray nozzle (bars)	3
Wire's speed (mm/s)	6
Generator voltage (V)	30
Current intensity (A)	100
Spray distance (mm)	140
Spray angle	90
Wire diameter (mm)	1.6

The development of the metal coatings required to use a gun flame-wire electric Arc spray 234 (Metal Spary Co. Ltd, Aukland, New Zealand). The thickness of this coating was approximately 600 µm. During projection, the gun is positioned perpendicular to the surface of the substrates at a controlled distance of about 150 mm. A compressed air jet located about 80 mm from the sample is directed to the surface of the deposit after the projection, to control cooling. The mechanical and physical properties of the used materials and the spray parameters used are given in *Table 4*and *Table 5*.

Table 5. Mechanical and physical properties of the used materials

Properties	ASTM 2017A	ASTM 5754	ASTM 301	75E
Elastic Modulus E (GPa)	72.5	70.5	200	187
Shear modulus (GPa)	27.2	26.5	76	70
Poisson ratio (ν)	0.33	0.33	0.29	0.32
Thermal expansion α (10^{-6} K^{-1})	22.9	23.7	16	11
Density ρ (Kg m^{-3})	2790	2680	7900	7130

2.2. Microstructural and Structural characterization

Microstructures of coatings were observed on a (QUANTA 600FEI) scanning electron microscope (SEM) coupled with energy dispersive X-ray analyzer, which allows a correspondence of image observation and chemical analysis. The coating thickness was measured by taking back scattered electron image (BSEI). The beam size is typically on the order of 1µm, and a typical detection limit is ≤ 1 at %, and thus, we anticipated that this method might provide information on the extent of homogenization achieved during the thermal spraying. Chemical composition of coatings was analyzed using an energy dispersive spectroscopy (EDS).

The X-ray diffraction patterns were recorded using diffractometer type X'PERT PRO MRD of PANalytical, equipped with a copper anode X-ray tube. The components Kα2 are not filtered by a monochromator graphite curve mounted in the secondary beam. The strong presence of defects in these materials creates a significant background noise; to improve counting statistics and increase the ratio pics/continuous background, an acquisition time of 40 s per angular step of 0.04 ° and a count time of 5s per step has been used in the interval ranging between 45° and 130°(2θ). The identification of the crystal phases present was made by comparison of the observed lines with those appropriate phases contained in the database PDF2.

2.3. Microhardness

Vickers microhardness profile of different multilayered materials have been made on coating (ASTM 301), bond coat (75E) and two different substrate (ASTM 5754, ASTM 2017A). Vickers microhardness was performed on the as-polished using semi-instrumented optical indenter Shimadzo MM1006. A test was carried out under a load of 250g load for 15 seconds. The value of the load was chosen to produce well-size imprints for better measurements and microhardness determination. An average hardness was calculated from 10 indents per specimen.

2.4. Mechanical Properties

Adhesion tensile tests were performed to measure the adhesive strength of the coating and substrate using a ZWICK/Rowell tensile-compression machine test system. A widely used adhesion test was the tensile adhesion test according to the ASTMC633 standard [42]. This test consists of a notch flexural beam. The specimen is a bi (or more) material beam with a central notch (*Figure 1*). In our case, the coating is stiff enough so that we do not have to glue a stiffener to enhance the delamination. Moreover, due to the brittle behavior of the coating, only a short notch is necessary to initiate fracture. The sample was placed on a device which was set up on a ZWICK/Roell tensile-compression machine. Tests are conducted with a constant displacement rate of 0.5 mm/min. Hence, a CCD camera allows recording beam cross-section all along its deformation.

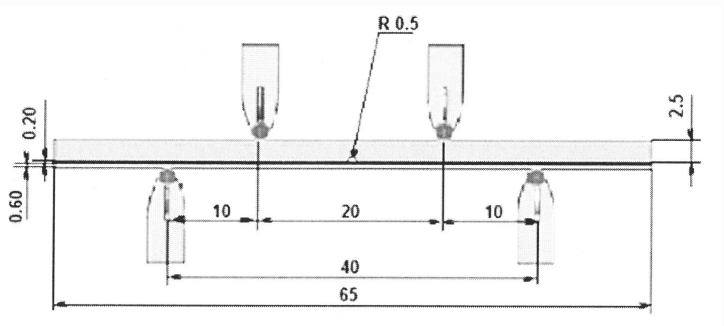

Figure 1. Four-point bending test used for adhesion measurements.

In order to follow the initiation and the propagation of the interfacial crack, a crack initiates at the notch, first in the coating and then propagates symmetrically in the coating-substrate interface. This crack is subject to constant moment conditions and propagates in steady state conditions. The strain energy release rate G_{IC} can be evaluated analytically using Euler–Bernoulli beam theory as following (Eq. (1)):

$$G_C = \frac{3}{2}\frac{P_C{}^2 l^2}{b^2 e^3}\frac{(1-\nu_S^2)}{E_S}\left[\frac{1}{\left(\frac{e_S}{e}\right)^3} - \frac{\lambda}{\left(\frac{e_d}{e}\right)^3+\lambda\left(\frac{e_S}{e}\right)^3+3\lambda\left(\frac{e_d e_S}{e^2}\right)\left(\frac{e_d}{e}+\lambda\frac{e_S}{e}\right)^{-1}}\right] \quad (1)$$

$$\lambda = \frac{E_S}{E_d}\frac{(1-\nu_d^2)}{(1-\nu_S^2)} \quad (2)$$

P_c is delamination strength (Newton); E_s is substrate Young's modulus (for ASTM5754 (69 GPa); for ASTM2017A (72 GPa); E_d is coating Young's modulus (90 GPa for ASTM301); ν_s is substrate Poisson's ratio (0.33 for both substrate); ν_d is deposit Poisson's ratio (0.34 for ASTM301); e_d is deposit thickness = 0.8 mm; e_s is substrate thickness = 2.5 mm; $e=e_s+e_d$; b is sample widths =10 mm; and l is distance between internal and external alumina blocks =10 mm. The fracture (or delamination) strength P_c is determined from the load displacement curve obtained during the test. It generally corresponds to a plateau, but in some case only an inflexion on the curve is observed.

3. RESULTS AND DISCUSSION

3.1. X-ray diffraction analysis (XRD)

The Structure of the ASTM 301 austenitic stainless steel coating and with the 75E as bond-coat is investigated by X-ray diffraction. The identification of the crystalline phases is made by comparison between the lines observed and those of the suitable phases contained in the data base PDF2. *The Figure 2* shows the diffractogram obtained exclusively from the ASTM 301 austenitic stainless steel.

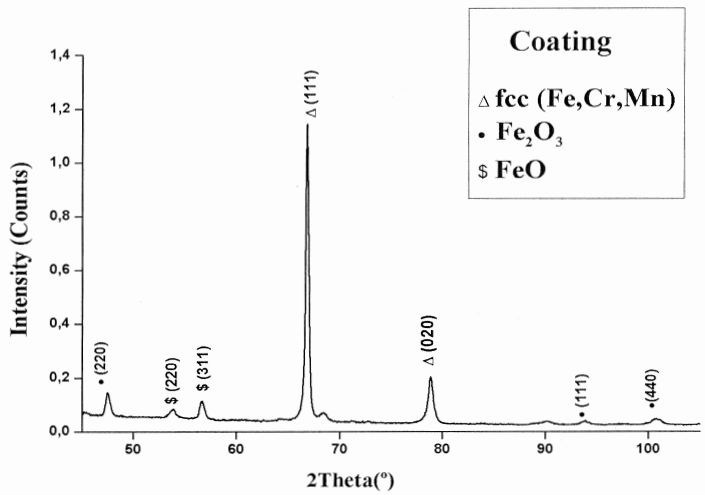

Figure 2. XRD spectrum of coating austenitic stainless steel ASTM 301.

The observed peaks are identified main phase as face-centered cubic (fcc) (Fe, Cr, Mn) structure with a lattice parameter of 3.5160 A° that corresponds to the solid solution (JCPDS n° 01-088-2327). The XRD spectrum of coating revealed also the presence of small proportion, of the metastable form γ-Fe_2O_3 (JCPDS n° 039-0238). One can also note the presence of FeO (JCPDS n° 028-0491). The formation of iron oxide FeO is due to the trapping of oxygen by the steel coating on the substrate; this oxygen then reacts with iron during cooling which leaves porosity in the texture.

3.2. Microstructure investigation

Figure 3 shows Typical SEM cross-sectional morphology of both ASTM 2017A/75E/ASTM 301 and ASTM 5754/75E/ASTM301 multilayered materials with typical lamellar steel splats, unmelted particles, oxides, inclusions, micro-cracks and pores. Unmelted particles are identified in the coating by their size and near-spherical morphology similar to that shown in Figure.3b. The oxides are probably formed due to the oxidation in-flight particles which appeared in the microstructure in the form of intersplat lamellae or globules oriented parallel to coating surface. The formation of micro-cracks confirms that the particles of the ASTM 301 stainless steel coating have several changes and distortion during coating. The microstructural observations of the interface between the substrate and the bond coat reveal a good adhesion of the sublayer with the coating although their respective coefficients of thermal expansion α are very different. Their ratio is approximately 2 since $\alpha=16\times10^{-6}$ K^{-1} for the austenitic stainless steel coating and 11×10^{-6} K. In addition, bond coat of the Ni base applied to the restoration of worn surfaces of crank pins and crankshaft bearings, can really be questioned since the linear dilatation coefficient of the austenitic

stainless steel coating (16×10^{-6} K^{-1}) is near to those of the bond coating 75 E (11×10^{-6} K^{-1}) and the two substrates ASTM 5754 ASTM 2017A (23×10^{-6} K^{-1}), (22.9×10^{-6} K^{-1}) respectively. The observation of micrographs exhibiting transverse sections reveals a perfect interface between the coating and the substrate.

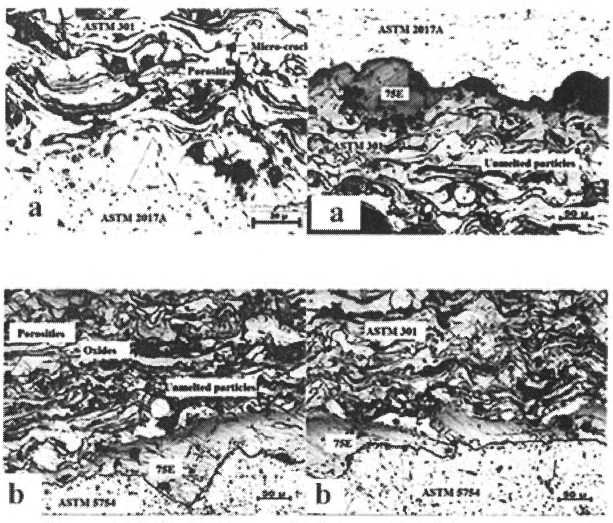

Figure 3. SEM (backscattering) of coatings: a) composite system A; b) composite system B.

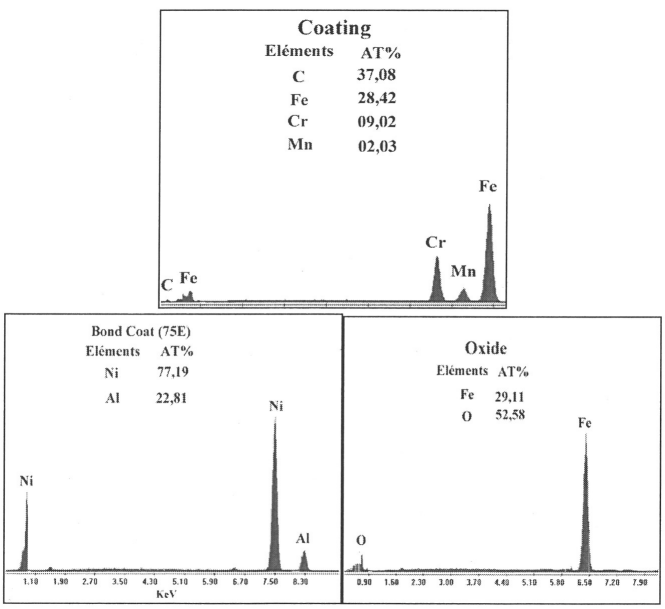

Figure 4. EDS analysis of the different phases of the stainless steel coating.

The results of EDS (Figure 4) indicated that the coating ASTM 301 is relatively formed by two phase one the main phase is the dark area identified as fcc (Fe, Cr, Mn) solid solution, while Ni dissolved in this fcc solid. We also note the presence of white nodules that represents oxides type Fe_xO_y wich is appeared in EDS analysis with different atomic ratio, this phase are mainly constituted by iron and large quantity of oxygen. In arc spray process, the formation of hard films such as Fe_xO_y oxide phase leads to improved mechanical properties [43, 44]. We can also remark that the lighter area of bond coat (75E) is uniform and homogenate. It was constituted by Ni and Al essentially.

3.3. Microhardness

The microhardnesses of the various materials used substrate ASTM 5754 and ASTM 2017A, bond coat E75, austenitic stainess steel ASTM 301 were measured by Vickers indentation with a load of 250 g during 15 seconds. For each processing, the calculated average standard deviation is based on the average of 20 measurements. The results of Vickers hardness are illustrated by the profil in *Figure 5*. These tests revealed that the microhardness measurements obtained for the two multimaterial shows the same evolution from the coating to the substrate surface. The microhardness of the ASTM 5754 and ASTM 2017A substrates were found in range of 63-68 $HV_{0.25}$ and 121-126 $HV_{0.25}$ respectively, whereas the microhardness of the 75E bond coat (250-350 $HV_{0.25}$) and ASTM 301 coatings (470-550 $HV_{0.25}$). The microhardeness of coatings is near four times than the two substrates. Therefore, this difference can be explained by the influence of the quantity of porosity and the homogenous of microstructure.

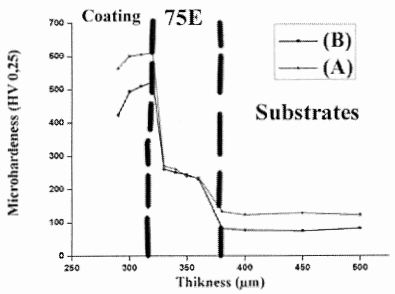

Figure 5. Microhardness profile of different system composite.

3.4. Coating adherence

As shown in Fig. 6, the curves of the load P against displacement u for all completed tests have a similar shape. With the increase of displacement u, P initially increases linearly, plateaus with some fluctuations and then increases again proportionately. A schematic of these curves is given in Fig. 7a where the various stages are identified and various points labeled. Over portion OA (1st stage), the coatings deform elastically accumulating strain energy for subsequent cracking. After this first stage, delamination of coating systems is observed beginning and propagation along interface when loads reach a certain critical value corresponding to one point near B in *Figure 6*. This interface crack then extends rapidly along the interface, corresponding to portion AB (2nd stage) in Fig. 7a. When cracks have propagated to distances and change paths and traverse the transition zone with some fluctuation wich is showed in figure 6. This latter process corresponds to

portion (3rd stage). Crack growth continues in a stable manner, corresponding to portion CD (4th stage).

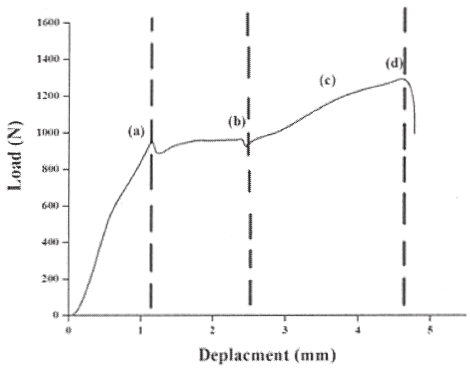

Figure 6. Load-displacement curve in the four-point bending.

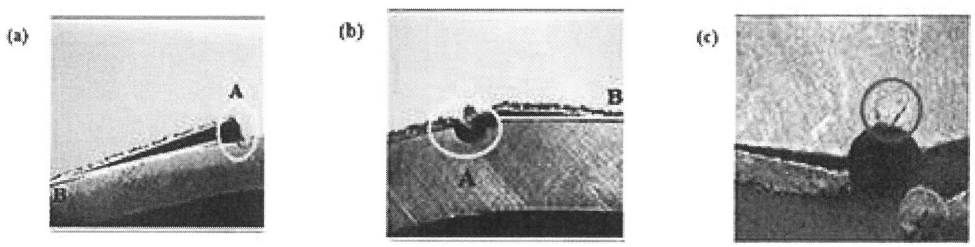

Figure 7. Microscopy Image of the cross-section of system composite interface delamination.

Figure 8 shows that the critical interfacial fracture energy G_{IC} of the composite system B under realized with bonding layer of Ni-Al is three times greater than the composite system A (260 ± 20J/m^2 against 110 ± 17J/m^2). In recent research [45] it found that the interfacial fracture energies of coating made without bond coat is about 11.4 J/m^2. The most favorable behavior is the composite system B, so the increase critical interfacial fracture energy G_{IC} promotes adhesion of the coating and increases the resistance to interfacial failure. This behavior can be explained by the presence of high compressive residual stress induced by grit blasted. It seems also from the results obtained that the chemical element substrate such the presence of copper strongly improves the adhesion of the stainless steel coating. Furthermore, the effect of the chemical nature of the sub bonding layer appears to be an important parameter for the adherence case of the stainless steel coating. All these results lead us to confirm the best performance of the composite system B compared with the composite system B. In recent research [45], the stainless steel deposits made without bond-coat of Ni-Al present cohesive delamination. In contrast, for the same coatings made with a bond-layer under the Ni-Al, delamination is adhesive with the presence of cracks.

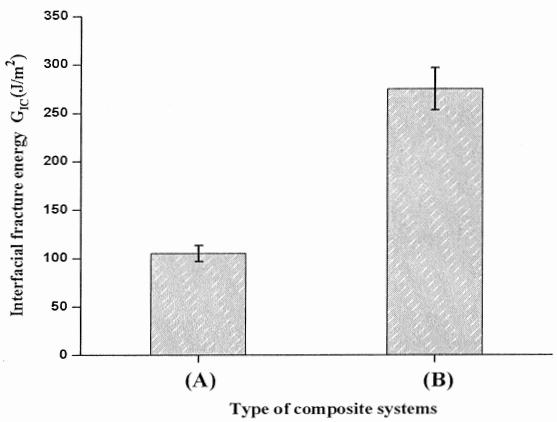

Figure 8. Variation of Interfacial fracture energy of composite systems (A): ASTM 5754/75 E bond coat/ASTM 301 and (B): ASTM 2017/75E bond coat/ASTM 301. Longitudinal bars show maximum and minimum of the measured fracture energy.

4. CONCLUSION

The aim of the present paper is to study the successful application of X10CrNi18-8 stainless steel (ASTM 301) coatings onto two different substrate aluminum alloys AG3 (ASTM 5754) and AU4G (ASTM 2017A) by using arc spraying process in order to improve the interfacial strength. On the basis of the obtained results in the present investigation, the following conclusions can be drawn:

- The SEM microstructures coatings showed that their morphology of both ASTM 2017A/75E/ASTM 301 and ASTM 5754/75E/ASTM 301 multilayered materials is constituted with typical lamellar steel splats, unmelted particles and porosities. The observations of the interface between the substrate and the bond coat reveal a good adhesion of the sublayer with the coating although their respective coefficients of thermal expansion α are different.

- The XRD spectrum of coating revealed the main phase corresponding the solid solution as face-centered cubic (fcc) (Fe, Cr, Mn) structure and also the presence of small proportion of the metastable form γ-Fe_2O_3 and FeO oxides.

- The microhardness of the ASTM 5754 and ASTM 2017A substrates were found in range of 63-68 $HV_{0.25}$ and 121-126 $HV_{0.25}$ respectively, whereas the microhardness of the 75E bond coat (250-350 $HV_{0.25}$) and ASTM 301 coatings (470-550 $HV_{0.25}$). The microhardeness of coatings is near four times than the two substrates.

- The 4-point bending tests results showed that the critical interfacial fracture energy G_{IC} of the composite system B realized with bonding layer of Ni-Al is three times greater than the composite system A.

5. REFERENCES

[1] A.R. Kelshami, A.A. Zadeh, M.M. Hadavi, A. Banerji, A. Alpas, A.P. Gerlich. Mater. Design. 86 (2015) 98.

[2] W. Tillmann, L. Hagen, D. Stangeier, I.A. Laemmerhirt, D. Biermann, P. Kersting, E. Krebs. Surf. Coat. Tech. 280 (2015) 16.

[3] Guoliang Hou, Yulong An, Xiaoqin Zhao, Huidi Zhou, Jianmin Chen, Acta Mater. 95 (2015) 164.
[4] Li Lin, Guo-Lu Li, Hai-Dou Wang, Jia-Jie Kang, Zhong-Lin Xu, Hai-Jun Wang, App. Surf. Sci. 356 (2015) 383.
[5] Li LU, Qi-min WANG, Bing-zhou CHEN, Yong-cui AO, Dong-hai YU, Cheng-yong WANG, Shang-hua WU, Kwang Ho KIM, Transactions of Nonferrous Metals Society of China 24 (2014) 1800.
[6] L. Hattali, S. Valette, S. Ropital, N. Mesrati, D. Treheux, J. Eur. Ceram. Soc. 29 (2009) 813.
[7] L. Hattali, S. Valette, S. Ropital, N. Mesrati, D. Treheux, Mater Sci, 44 (2009) 3198.
[8] J.C. Avelar , B. Wilson, S. Wu, I. Gotman, J. Housden , E.Y. Gutmanas, Mater. Lett. 157 (2015) 45.
[9] Yuta Watanabe , Chisato Yoshida, Keisuke Atsunami, Motohiro Yamada, Masahiro Fukumoto, J. Therm. Spray Techn. 24 (2015) 86.
[10] A. Miletic, P. Terek, L. Kovacevic, M. Vilotic, D. Kakas, S. Branko, D. Kukuruzovic, Journal of the Brazilian Society of Mechanical Sciences and Engineering , 36 (2014) 293.
[11] D.M. Karpinos, V.G. Zil'berberg, Soviet Powder Metallurgy and Metal Ceramics, 12 (1973) 815.
[12] G.H.S Gava, R.M.D. Souza , J.D.B. de Mello, M.C.S de Macedo, C. Scandanian, Wear, 301 (2013) 130.
[13] D. Bhattacharjee, K. Muthusamy, S. Ramanujam, Tribol. T., 57 (2014) 292.
[14] A. Pramanik, G. Littlefair, Mach. Sci. Technol. 19 (2015) 1.
[15] A. Pramanik, L.C. Zhang, Y.Q. Chen. Advanced Materials Research 97 (2010) 2269.
[16] L.C. Zhang, E. Kiat, A. Pramanik. Advanced Materials Research 76 (2009) 212.
[17] J. Chen, S.J. Bull, J. Phys. D Appl. Phys. 44 (2011) 34.
[18] J. Chen, Z.S. Lin, S.J. Bull, C.L. Phillips, P.D. Bristowe, J. Phys. D Appl. Phys. 42 (2009) 21.
[19] R.E. Galindo, A. Veen, J.H. Evans, H. Schut, J. Hsson, Thin Solid Films 471 (2005) 170.
[20] J. Ding, Y. Meng, S. Wen, Thin Solid Films 371 (2000) 178.
[21] P.C. Jindal, D.T. Quinto, G.J. Wolfe, Thin Solid Films 154 (1987) 361.
[22] D.B. Marshall, A.G. Evans, J. Appl. Phys. 56 (1984) 2632.
[23] M.B. Modi, S.K. Sitaraman, Eng. Fract. Mech. 71 (2004) 1219.
[24] M. Uhlig, A. Bertz, M. Rennau, S.E. Schulz, T. Werner, T. Gessner, J. Microelectron.Eng. 50 (2000) 7.
[25] L.Y. Huang, K.W. Xu, J. Lu, Diamond Relat. Mater. 11 (2002) 1505.
[26] D. Dalmas, E. Barthel, D. Vandembroucq, J. Mech. Phys. Solids 57 (2009) 446.
[27] E. Barthel, O. Kerjan, P. Nael, N. Nadaud, Thin Solid Films 473 (2005) 272.
[28] V. Gupta, J. Yuan, A. Pronin, J. Adhes. Sci. Technol. 8 (1994) 713.
[29] M. Zhou, Y.K. Zhang, L. Cai, Appl. Phys. A: Mater. Sci. Process. 74 (2002) 475.
[30] T. An, F. Qin, J. Li, Microelectron. Reliab. 51 (2011) 1011.
[31] O.M. Abdelhada, L. Ladania, J. Razmib, Mech. Mater. 43 (2011) 885.
[32] X. Chen, Y.C. Lin, X. Liu, G.Q. Lu, Eng. Fract. Mech. 72 (2005) 2628.
[33] K.R. Gadelrab, M. Chiesa, M. Hecker, H.J. Engelmann, Eng. Fract. Mech. 96 (2012) 490.
[34] S. Roham, T. Hight, Microelectron. Eng. 84 (2007) 72.
[35] S. Roham, K. Hardikar, P. Woytowitz, J. Mater. Res. 19 (2004) 3019.
[36] Z. Gan, S.G. Mhaisalka, Z. Chen, K. Prasad, S. Zhang, M. Damayanti, N. Jiangd, J. Electrochem. Soc. 153 (2006) G30.
[37] Z. Gana, S.G. Mhaisalkara, Z. Chena, S. Zhangb, Z. Chenc, K. Prasadc, Surf. Coat. Tech. 198 (2005) 85.
[38] M.P. Hughey, D.J. Morris, R.F. Cook, S.P. Bozeman, B.L. Kelly, S.L.N. Chakravarty, D.P.Harkens, L.C. Stearns, Eng. Fract. Mech. 71 (2004) 245.
[39] D.M. Gage, K. Kim, C.S. Litteken, R.H. Dauskardt, J. Mater. Res. 23 (2008) 87.

[40] C.C. Lee, Surf. Coat. Tech. 215 (2013) 400.
[41] C.C. Lee, J. Huang, S.T. Chang, W.C. Wang, Thin Solid Films 517 (2009) 4875.
[42] Standard Test Method for Adhesion or Cohesion Strength of Thermal Spray Coatings, ASTM Standard C 633-01, ASTM, West Conshocken, PA, USA, 2001.
[43] R. Viana, M.S.F. Lima, W.F. Sales, W.M. Da Silva, R. Machadoa. Surf. Coat. Technol. 276 (2015) 485.
[44] O. Takakuwa, H. Soyama, Surf. Coat. Tech. 206 (2012) 3747.
[45] M. Laribi, N. Mesrati , A.B. Vannes , D. Treheux, Surf. Coat. Tech. 166 (2003) 206.

(Article reçu le 17/12/2016, sous forme définitive le 22/12/2016.